

Manipulating the Cellular Circadian Period of Arginine Vasopressin Neurons Alters the Behavioral Circadian Period

メタデータ	言語: eng 出版者: 公開日: 2017-10-03 キーワード (Ja): キーワード (En): 作成者: メールアドレス: 所属:
URL	http://hdl.handle.net/2297/46537

Manipulating the Cellular Circadian Period of Arginine Vasopressin Neurons Alters the Behavioral Circadian Period

Michihiro Mieda¹, Hitoshi Okamoto², Takeshi Sakurai^{1,3}

¹Department of Molecular Neuroscience and Integrative Physiology, Faculty of Medicine, Kanazawa University, 13-1 Takara-machi, Kanazawa, Ishikawa 920-8640, Japan.

²Laboratory for Developmental Gene Regulation, RIKEN Brain Science Institute, 2-1 Hirosawa, Wako, Saitama 351-0198, Japan.

³Present address: International Institute for Integrative Sleep Medicine, University of Tsukuba, Tsukuba, 305-8575, Japan

Corresponding author:

Dr. Michihiro Mieda, Department of Molecular Neuroscience and Integrative Physiology, Faculty of Medicine, Kanazawa University, Kanazawa, Ishikawa 920-8640, Japan; Email: mieda@med.kanazawa-u.ac.jp

Manuscript information: 4 figures, 4 supplemental figures, 4 supplemental tables, 1 supplemental experimental procedures

SUMMARY

As the central pacemaker in mammals, the circadian clock in the suprachiasmatic nucleus (SCN) of the hypothalamus is a heterogeneous structure consisting of multiple types of GABAergic neurons with distinct chemical identities [1, 2]. Although individual cells have a cellular clock driven by autoregulatory transcriptional/translational feedback loops of clock genes, interneuronal communication among SCN clock neurons is likely essential for the SCN to generate a highly robust, coherent circadian rhythm [1]. However, neuronal mechanisms that determine circadian period length remain unclear. The SCN is composed of two subdivisions: a ventral core region containing vasoactive intestinal peptide (VIP)-producing neurons and a dorsal shell region characterized by arginine vasopressin (AVP)-producing neurons. Here, we examined whether AVP neurons act as pacemaker cells that regulate the circadian period of behavior rhythm in mice. The deletion of *casein kinase 1 delta (CK1 δ)* specific to AVP neurons, which was expected to lengthen the period of cellular clocks [3-6], lengthened the free-running period of circadian behavior as well. Conversely, the overexpression of *CK1 δ* specific to SCN AVP neurons shortened the free-running period. PER2::LUC imaging in slices confirmed that cellular circadian periods of the SCN shell were lengthened in mice without *CK1 δ* in AVP neurons. Thus, AVP neurons may be an essential component of circadian pacemaker cells in the SCN. Remarkably, the alteration of the shell–core phase relationship in the SCN of these mice did not impair the generation per se of circadian behavior rhythm, thereby underscoring the robustness of the SCN network.

RESULTS

***CK1δ* deficiency in AVP neurons lengthens, while its overexpression shortens, the free-running period of circadian behavior rhythm**

To test whether AVP neurons actively work as pacemaker cells to regulate the circadian period in mice, we assessed whether genetic manipulations of *CK1δ* expressions in AVP neurons alter the period of behavior rhythm. In doing so, we acknowledged that the phosphorylation of PER proteins by CK1δ might enhance those proteins' degradation and consequently accelerate the speed of cellular clocks [7-13]. Indeed, the deletion of *CK1δ* has been reported to lengthen periods of PER2::LUC oscillation by 1.5–3 hr [3-6].

To generate mice lacking functional CK1δ specifically in AVP neurons, we crossed *Avp-Cre* mice [14] that express improved Cre recombinase specifically in AVP neurons with mice carrying floxed *CK1δ* alleles (*CK1δ^{lox2/flox2}*) [3], hereafter designated as *Avp-CK1δ^{-/-}* mice. In 12 hr of light and 12 hr of darkness (LD), *Avp-CK1δ^{-/-}* mice showed diurnal rhythm of spontaneous locomotor activity comparable to control mice (*CK1δ^{lox2/flox2}* and *Avp-Cre;CK1δ^{+/flox2}* mice) (Figure 1; Tables S1 and S2). By contrast, in constant darkness (DD), *Avp-CK1δ^{-/-}* mice free-ran with a period approximately 50 min longer than that of control mice (24.72 ± 0.03 hr versus 23.94 ± 0.03 hr, $p < 0.001$), while their activity time remained normal (13.96 ± 0.19 hr versus 13.42 ± 0.21 hr, $p = 0.231$).

Conversely, *Avp-CK1δ^{-/-}* mice with *CK1δ* overexpression in the SCN AVP neurons (*Avp-CK1δ^{-/-}+AAV-DIO-CK1δ* mice)—achieved via focal injection of Cre-dependent adeno-associated viral (AAV) expression vectors in adult mice—free-ran

with a period approximately 30 min shorter than that of control mice (23.46 ± 0.06 hr, $p < 0.001$) (Figures 1 and S1; Table S2). The depression of activity level in *Avp-CK1 δ ^{-/-}+AAV-DIO-CK1 δ* mice were likely due to AAV injections, because that was observed also in control mice for the surgery (*Avp-CK1 δ ^{-/-}+AAV-DIO-mCherry* mice, Table S2).

Collectively, the manipulation of *CK1 δ* expression levels in AVP neurons of the SCN bidirectionally changed the free-running period of behavior rhythm.

***Avp-CK1 δ ^{-/-}* mice respond to an 8-hr phase advance of the LD cycle by delaying their behavior rhythm**

When the 8-hr phase advance of LD cycle was given, in clear contrast to control mice (8 of 8 mice), the *Avp-CK1 δ ^{-/-}* mice reentrained to the new LD cycle by delaying their activity rhythm (7 of 7 mice) (Figure S2A). The number of days required for reentrainment was significantly fewer in *Avp-CK1 δ ^{-/-}* mice when the LD cycle was advanced but not when it was delayed (phase advance: 8.25 ± 0.41 days versus 11.75 ± 0.90 days, $p < 0.01$; phase delay: 5.71 ± 0.47 days versus 5.62 ± 0.32 days, $p = 0.876$) (Figure S2B). This result was consistent with the lengthened circadian period of *Avp-CK1 δ ^{-/-}* [15, 16].

The phase-shifts of activity rhythms evoked by light pulses at CT14 and CT22 were comparable between control and *Avp-CK1 δ ^{-/-}* mice (Figures S2H and S2I).

Spatiotemporal pattern of gene expression changes in the SCN of *Avp-CK1 δ ^{-/-}* mice

We next evaluated the status of the molecular clock in the SCN by way of in situ hybridization (Figure 2). In the SCN of control mice, as expected, *Avp* mRNA was expressed predominantly in the shell and showed clear circadian expression, with a peak at approximately 20 hr in darkness (i.e., around CT8). The peak level of *Avp* mRNA expression in *Avp-CKI δ ^{-/-}* mice was similar to that in control mice. However, the increase in expression was significantly delayed in *Avp-CKI δ ^{-/-}* mice. The peak level of *Per1* mRNA expression, which is a core component of circadian clocks, was also similar between two groups in both the SCN shell and core. Intriguingly, the increase of *Per1* expression in the shell was significantly delayed relative to that of the core in *Avp-CKI δ ^{-/-}* mice. The clearest difference occurred at 16 hr in darkness (i.e., around CT4) (Figure 2B). Thus, the *CKI δ* deletion specific to AVP neurons might reorder the spatiotemporal pattern of gene expression in the SCN. The delay of gene expression in the shell of *Avp-CKI δ ^{-/-}* mice was consistent with the presumed lengthening of cellular periods in AVP neurons.

Deletion of *CKI δ* in AVP neurons lengthens cellular periods of the SCN shell and alters the spatiotemporal order of PER2::*LUC* oscillations in the SCN

Because *Avp-CKI δ ^{-/-}* mice free-ran with a coherently lengthened period, we expected that the cellular clocks of the entire SCN would also oscillate with a lengthened period. To test this hypothesis, we performed real-time bioluminescent cell imaging of coronal SCN slices prepared from control and *Avp-CKI δ ^{-/-}* adult mice with a luciferase reporter (*Per2::*Luc**) [17] housed in DD (Figures 3 and S3A; Table S3). Contrary to our expectations, the SCN

shell and core of *Avp-CK1 $\delta^{-/-}$;Per2::*Luc** mice transiently showed different cellular periods ex vivo (Figures 3A and 3C). The period of the shell was longer by approximately 2 hr at the beginning (shell: 25.91 ± 0.50 hr versus core: 23.73 ± 0.07 hr, $p < 0.001$) (Figure 3C and Table S3). However, this lengthening did not continue into the next cycle (shell: 23.65 ± 0.33 hr versus core: 23.98 ± 0.06 hr, $p = 0.343$). Accordingly, the peak time of PER2::*LUC* oscillation in the shell was later relative to that of the core at the first peak in *Avp-CK1 $\delta^{-/-}$;Per2::*Luc** mice (Figures 3A and 3D). This delay increased at the second peak, but did not increase any further in subsequent cycles. The peak amplitude of PER2::*LUC* oscillation was significantly lower and decayed more rapidly in the SCN shell of *Avp-CK1 $\delta^{-/-}$;Per2::*Luc** mice (Figures 3A and 3E; Table S3). These data suggest that intercellular communications between the shell and core somehow precluded the lengthening of shell's period in the prolonged culture.

We expected that blocking intercellular communications by the application of tetrodotoxin (TTX), a blocker of voltage-dependent sodium channels, would allow the core and shell regions to each express their endogenous period lengths ex vivo [18, 19]. Surprisingly, however, the transient period difference, followed by period length synchronization, persisted despite the application of TTX in the SCN slices of *Avp-CK1 $\delta^{-/-}$;Per2::*Luc** mice (Figures S3B and S4A-D; Table S3).

By extension, we aimed to reduce intercellular communications between the core and shell by surgically cutting the SCN slice along the horizontal plane (Figures 3B, S3C, and S3D; Table S3). In slices with knife cuts, the lengthened period of the SCN shell in *Avp-CK1 $\delta^{-/-}$* mice was maintained for a longer duration (Figure 3F and Table S3).

Accordingly, the peak time difference of PER2::LUC oscillation between the shell and core increased linearly for three cycles (Figure 3G). This result suggested that the core sent a signal that modulated the shell in the SCN slices, which was attenuated by surgical cuts between the regions. Such data indicate that the periods of cellular clocks in the SCN shell were lengthened in *Avp-CK1 δ ^{-/-}* mice by 1.4–2 hr.

To increase the resolution of circadian rhythm analysis, we applied a cosine curve-fitting method on PER2::LUC oscillations in individual pixels that covered the SCN (Figures 4 and S4E–G; Table S4)[20]. The periods of pixels in the shell were lengthened in *Avp-CK1 δ ^{-/-}* mice, which was more obvious in slices with surgical cuts (Figures 4A, 4C and S4E). In control mice, we observed phase-leading cells (i.e., pixels) located dorsomedially [19], whose first acrophase (peak phase) was advanced relative to other pixels. However, such phase-leading cells were not clearly found in *Avp-CK1 δ ^{-/-}* mice. Raster plots of signal intensity across the SCN further demonstrated that dorsomedial pixels were phase-advanced in control mice, whereas those in *Avp-CK1 δ ^{-/-}* mice were obviously phase-delayed relative to the pixels in the core (Figures 4B, 4D and S4F). The phase delay continued to increase in slices with surgical cuts, yet not in intact or TTX-treated slices, as observed in ROI analyses described above (Figures 3 and S4). These data suggest that the spatiotemporal pattern of PER2::LUC oscillation throughout the SCN was altered in *Avp-CK1 δ ^{-/-}* mice, a conclusion consistent with results of gene expression in vivo elucidated by in situ hybridization (Figure 2).

The mean period of individual pixel oscillations was significantly lengthened by 2–2.5 hr in the shell of *Avp-CK1 δ ^{-/-}* mice (Figures 4E, 4F and S4G; Table S4). Interestingly,

when the cumulative frequency of the pixel periods was plotted, we found a peak of pixels with normal periods in slices with surgical cuts, which was smoothed in intact and TTX-treated slices (Figures 4E, 4F, and S4G). This peak might represent non-AVP neurons and a small number of AVP neurons that sustain an undeleted *CK1 δ* allele. This observation further supported a notion that the intercellular interaction modified the cellular periods of the shell. The mean first acrophase of the individual pixel oscillations was delayed in the shell by 2–3 hr compared to that of the core (Figures 5E, 5F, S4G, and Table S4). It should be noted that TTX application indeed altered some aspects of the SCN network property, such as the first acrophase of pixels in the core of both control and *Avp-CK1 δ ^{-/-}* mice (Figure S4G).

Collectively, these data suggest that periods of cellular clocks in the SCN shell were lengthened in *Avp-CK1 δ ^{-/-}* mice by roughly 2 hr, which altered the spatiotemporal pattern of PER2::LUC oscillation across the SCN.

DISCUSSION

We recently demonstrated that mice with a *Bmal1* deletion specific to AVP neurons (*Avp-Bmal1^{-/-}* mice) showed marked lengthening and instability in the free-running period and activity time of behavior rhythm [14]. This result suggested that cellular clocks in AVP neurons are required for the appropriate, stable expression of the circadian period by enhancing the coupling of SCN neurons. However, the relative contribution of the loss of synchronizing signals versus the loss of rhythmicity in AVP neurons was inseparable. By extension, the present study provides clear evidence that AVP neurons indeed regulate SCN

pacemaking. It is unlikely that the AVP peptide solely mediates this effect, because a deficiency of AVP signaling does not change the free-running period in mice or rats [21, 22]. Interestingly, the alteration of the shell–core phase relationship did not impair the generation per se of behavioral circadian rhythm, thereby indicating the robustness of the SCN network. It should be emphasized that the circadian phenotype of *Avp-Bmal1*^{-/-} mice was not identical to that of *Avp-CK1δ*^{-/-} mice, making it unlikely that *CK1δ* deletion disrupted the cellular clock beyond simply altering the period.

Wild-type↔*Clock*^{Δ19/Δ19} mutant chimera mice in which random subsets of wild-type SCN cells were replaced with *Clock*^{Δ19/Δ19} cells demonstrated a number of intermediate circadian phenotypes [23]. Notably, their circadian period and amplitude were highly labile, which contrasted those of *Avp-CK1δ*^{-/-} mice. Such a qualitative difference may indicate a specialized role for AVP neurons in SCN pacemaking.

Lee et al. employed an approach similar to ours. They demonstrated that the free-running period of behavior was extended by lengthening the cellular period of neuromedin S (NMS)-producing neurons by way of the overexpression of *Clock*^{Δ19} [24]. NMS neurons represent a heterogeneous population with AVP and VIP neurons, among other neuronal types [24]. Surprisingly, overexpression of the *Clock*^{Δ19} transgene in VIP neurons had no effect on the behavioral free-running period [24]. Indeed, VIP has been demonstrated to be especially important for the maintenance and synchronization of cellular clocks in individual SCN neurons [25-28].

More recently, Smyllie et al. created chimeric mice with SCN containing dopamine 1a receptor (*Drd1a*) cells with an intrinsic cellular period of 24 hr alongside

non-Drd1a cells with a period of 20 hr [18]. Remarkably, 60% of chimeric mice showed 24-hr periods of behavior and SCN PER2::LUC rhythms, whereas 33% showed 20-hr periods. Moreover, the chimeric SCN sustained a wave of PER2::LUC bioluminescence comparable to that of nonchimeric SCN. These characteristics contrast starkly with those of *Avp-CK1 δ ^{-/-}* mice. Drd1a cells contain 63% of all SCN cells, including 62% of AVP neurons and 81% of VIP neurons, though <1% of GRP neurons [18]. Therefore, the slight difference in the ratio of 24-hr AVP neurons to 20-hr AVP neurons could exert a substantial impact on the period with which the chimeric SCN oscillates. However, our results suggest that AVP neurons alone cannot set the normal spatiotemporal order of circadian oscillation across the entire SCN. Accordingly, AVP neurons might need to work in concert with other types of neurons to reorganize the entire SCN network. In contrast to AVP neurons, as Lee et al. and Smyllie et al. both indicated, genetic manipulations that lengthen the cellular period in most VIP neurons do not change the speed of the SCN. Cellular clocks in VIP neurons and other types of non-AVP neurons might stabilize the circadian oscillation of the entire SCN, which could support the robustness of the network.

PER2::LUC imaging suggested that cells in the SCN shell oscillated with periods of roughly 26 hr, whereas those in the core oscillated with periods of roughly 24 hr in *Avp-CK1 δ ^{-/-}* mice. However, the intrinsic period of the cellular clocks in AVP neurons measured in this study might be imprecise. Although AVP neurons represented the SCN shell, it also contained non-AVP neurons. Intercellular communications could have further affected the period of AVP neurons. Nevertheless, the roughly 2-hr difference of periods between shell and core oscillations concurs with values reported for *CK1 δ* -deficient cells

[3-6]. Unfortunately, we have no information concerning the behavioral free-running period of *CK1 δ ^{-/-}* mice, which died perinatally [3]. The behavioral free-running period of *Avp-CK1 δ ^{-/-}* mice was ~25 hr or between cellular periods of the SCN shell and core estimated from PER2::LUC imaging. Thus, coupling between AVP neurons and non-AVP neurons is likely to occur in vivo in determining the free-running period.

In this context, it is notable that surgical cuts between the shell and core stabilized the lengthened period of the shell in SCN explants of *Avp-CK1 δ ^{-/-}* mice, which implied a modulatory influence of the core on the period of the shell (Figures 3 and 4). Collectively, the core and shell may be held together in vivo by coupling, which is slightly less effective ex vivo, and thereby allow the core and shell to oscillate independently. During prolonged culture, the core and shell might settle into a new steady state with a stable period and phase relationship by way of intercellular communications. The emergence of a novel steady state of circadian oscillation in prolonged culture was also reported, even for the SCN of *Bmal1*-deficient mice [29]. Consequently, the intact structure of the SCN or its connections with extra-SCN regions, if not both, might be indispensable for such coupling in vivo, as our previous study implied [14]. The oscillation in the shell of *Avp-CK1 δ ^{-/-}* mice was dampened rapidly ex vivo (Figures 3, 4E and S4), whereas that in vivo did not show a reduction in its amplitude (Figure 2). This fact may suggest that the core-to-shell connection might be resistant while the shell-to-core connection might be more susceptible to slicing.

Surprisingly, TTX application did not erase the core's modulatory influence on the PER2::LUC period of the shell, for TTX is thought to disrupt interneuronal

communication [18, 19]. In fact, TTX application altered some aspects of PER2::LUC oscillations (Figure S4). We used SCN explants prepared from adult mice. Compared to SCN explant cultures from neonates [18, 19], SCN cultures from adults have shown gene expression with a far less drastic effect of TTX treatment [30]. Differences in the network properties of neonatal and adult SCN have been also reported [31]. Therefore, both sodium spike-dependent and -independent mechanisms of interneuronal communication are possible in the SCN of adult mice [32].

EXPERIMENTAL PROCEDURES

Animals

To generate *Avp-CK1 δ ^{-/-}* mice, *Avp-Cre* mice [14] were mated to mice with a conditional *CK1 δ* allele (*CK1 δ ^{flox2}*) [3]. All experimental procedures involving animals were approved by the appropriate institutional animal care and use committee of Kanazawa University.

Behavioral Analyses

Male and female *Avp-CK1 δ ^{-/-}* (*Avp-Cre;CK1 δ ^{flox2/flox2}*) and control (*CK1 δ ^{flox2/flox2}* and *Avp-Cre;CK1 δ ^{+ /flox2}*) mice were housed individually in a cage placed in a light-tight chamber. Spontaneous locomotor activity was monitored by infrared motion sensors in 1-min bins. Actogram, activity profile, and χ^2 periodogram analysis was performed via ClockLab (Actimetrics).

Bioluminescence Imaging

The *Avp-CK1 δ ^{-/-}* mice were further mated with *Per2::Luc* reporter mice [17]. Mice were housed in DD for 6 days before sampling. Coronal SCN slices of 150 μ m were cultured as described previously with slight modifications [33]. Images were acquired every 30 min and were analyzed using ImageJ and custom-made program [20].

SUPPLEMENTAL INFORMATION

Supplemental Information includes Supplemental Experimental Procedures, four figures, and four tables.

AUTHOR CONTRIBUTIONS

M.M. conceived and performed experiments, wrote the manuscript, and secured funding.

M.M. and H.O. provided resources. T.S. provided expertise and feedback.

ACKNOWLEDGEMENTS

This study was supported in part by MEXT KAKENHI Grants Number 24390052, 15K15039, 16H05120 and 16H01608; by the Takeda Science Foundation; by the Brain Science Foundation; and by the Ichiro Kanehara Foundation (M.M.). We thank D. Ono and S. Honma for technical advice on PER2::LUC imaging; D. R. Weaver for the *CK1 δ ^{flox2/flox2}* mouse; J. Takahashi for the *Per2::Luc* reporter mouse; K. Deisseroth for *pAAV-DIO-hChR2(H134R)-EYFP-WPRE-pA*; B. Roth for *pAAV-DIO-mCherry*; I. Kameshita for *pcFLAG-CK1 δ* ; and Penn Vector Core for *pAAV2-rh10*.

FIGURE LEGENDS

Figure 1. *Avp-CK1 δ ^{-/-}* mice show lengthening of the free-running period in DD. (A) Representative locomotor activity of control, *Avp-CK1 δ ^{-/-}*, and *Avp-CK1 δ ^{-/-}* mice overexpressing *CK1 δ* in SCN AVP neurons (*Avp-CK1 δ ^{-/-}*+AAV-*DIO-CK1 δ*). Gray shading indicates the time when lights were off. (B) Daily profile of locomotor activity in LD or DD. (C) Free-running period was lengthened in *Avp-CK1 δ ^{-/-}* mice and was shortened in *Avp-CK1 δ ^{-/-}*+AAV-*DIO-CK1 δ* mice. Error bars indicate S.E.M; n = 14 for control, n = 13 for *Avp-CK1 δ ^{-/-}* mice, and n = 8 for *Avp-CK1 δ ^{-/-}*+AAV-*DIO-CK1 δ* mice; ***, p < 0.001 versus control; ^^^, p < 0.001 versus *Avp-CK1 δ ^{-/-}*. (D) Representative images of mCherry expression in the SCN of *Avp-CK1 δ ^{-/-}*+AAV-*DIO-CK1 δ* mice injected with a mixture of recombinant AAV vectors expressing *CK1 δ* or *mCherry* in a Cre-dependent manner. Scale bars, 500 μ m for left panel; 100 μ m for right magnified panel. HDB, nucleus of the horizontal limb of the diagonal band; SON, supraoptic nucleus. See also Figures S1 and S2; Tables S1 and S2.

Figure 2. Circadian gene expression is delayed in the shell of SCN in *Avp-CK1 δ ^{-/-}* mice. (A) Representative images of *Avp* and *Per1* mRNA expression in the SCN of control and *Avp-CK1 δ ^{-/-}* mice at times indicated in darkness after the onset of the last dark phase (“12 hr” corresponds roughly to CT0). Coronal brain sections were hybridized in situ to an antisense probe for each gene. Scale bar, 100 μ m. (B) Circadian expression of each gene in the middle SCN along the rostral-caudal axis. Expression was quantified for the entire

section (*Avp*) or separately for the shell and core (*Per1*). Representative regions defined as the shell and core SCN are indicated by yellow circles in (A). Error bars indicate S.E.M; n = 6. g, effect of genotype in each region; r, effect of region in each genotype; by post hoc pairwise comparisons; lowercase, $p < 0.01$; italicized lowercase, $p < 0.05$.

Figure 3. The period of cellular circadian oscillation is lengthened in the shell of SCN in *Avp-CK1 δ ^{-/-}* mice. (A) Representative images of PER2::LUC expression. Coronal SCN slices of the mid-rostrocaudal region were prepared from adult control and *Avp-CK1 δ ^{-/-}* mice with a luciferase reporter (*Per2::Luc*) housed in DD. Detrended bioluminescence within the two shell and two core regions indicated in the images were plotted on the right. Gray vertical lines labeled “Day 1” indicate 15 hr after the start of image recordings around CT9. (B) SCN slices received surgical cuts along the horizontal plane, shown by arrows in the bright-field images on the left. (C, F) Periods of PER2::LUC oscillations for two cycles defined in (A). (D, G) Peak time differences between the shell and core of the SCN. (E, H) Amplitudes of the three peaks defined in (A). Data of SCN slices without (C–E) or with (F–H) surgical cuts. The period was clearly lengthened in the SCN shell of *Avp-CK1 δ ^{-/-};Per2::Luc* mice when slices received surgical cuts. Error bars indicate S.E.M; n = 5 for control, n = 7 (C–E) or 5 (F–H) for *Avp-CK1 δ ^{-/-};Per2::Luc* mice. For (C, D, F, G), G, effect of genotype in each region for each cycle; R, effect of region in each genotype for each cycle; C, effect of cycle (versus 2nd) in each region of each genotype; by post hoc pairwise comparisons. For (E, H), G, effect of genotype in the shell; R, effect of region in *Avp-CK1 δ ^{-/-}* mice; G x C, interaction between genotype and cycle in the shell; R x C,

interaction between region and cycle in *Avp-CK1 δ ^{-/-}* mice; by two-way repeated-measures ANOVA; uppercase, $p < 0.001$; lowercase, $p < 0.01$; italicized lowercase, $p < 0.05$. See also Figures S3 and S4; Table S3.

Figure 4. Spatiotemporal pattern of PER2::LUC oscillation is altered in the SCN of *Avp-CK1 δ ^{-/-}* mice. (A, C) Representative amplitude, period, and first acrophase maps of PER2::LUC oscillation at the pixel level of intact (A) or surgically cut (C) SCN slices shown in Figure 3. Amplitudes, periods, and acrophases of PER2::LUC oscillations in the individual pixels covering the SCN were calculated by cosine curve fittings for data representing 72 hr from the first CT6 after slice preparation, determined according to behavioral free-running period before slice preparation. For the first acrophase, “6 hr” corresponds to the beginning of cosine curved-fitted data at roughly CT6. (B, D) Raster plots of signal intensity from the dorsal tip to the end of ventral region as indicated by red lines in (A) and (C). (E, F) Mean and cumulative frequency of amplitude, period and first acrophase of individual pixels’ PER2::LUC oscillations. Cumulative frequency plots show the distribution of pixels’ periods and first acrophases. The dorsal 40% and ventral 30% regions of the SCN were regarded as the shell and core, respectively. Representative regions defined as the SCN shell or core are indicated in (A) and (C). Data of SCN slices without (E) or with (F) surgical cuts. Error bars indicate S.E.M; $n = 5$ for control, $n = 7$ (E) or 5 (F) for *Avp-CK1 δ ^{-/-};Per2::Luc* mice. G, effect of genotype in each region; R, effect of region in each genotype; by post hoc pairwise comparisons; uppercase, $p < 0.001$; lowercase, $p < 0.01$; italicized lowercase, $p < 0.05$. See also Figures S3 and S4; Table S4.

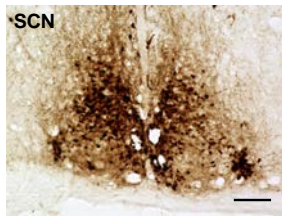
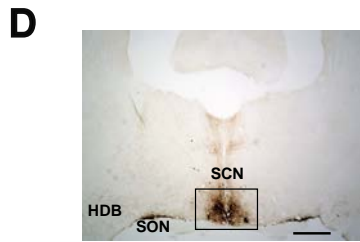
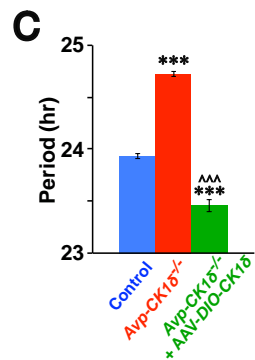
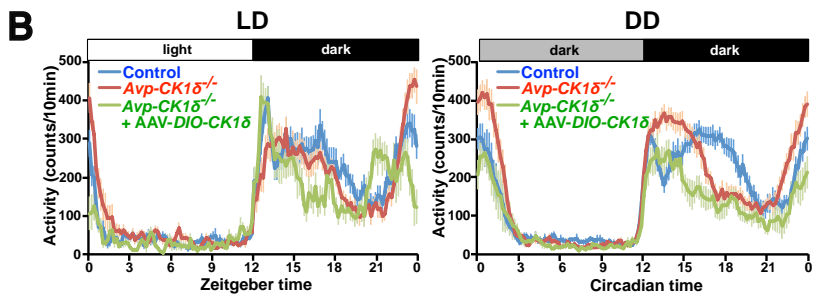
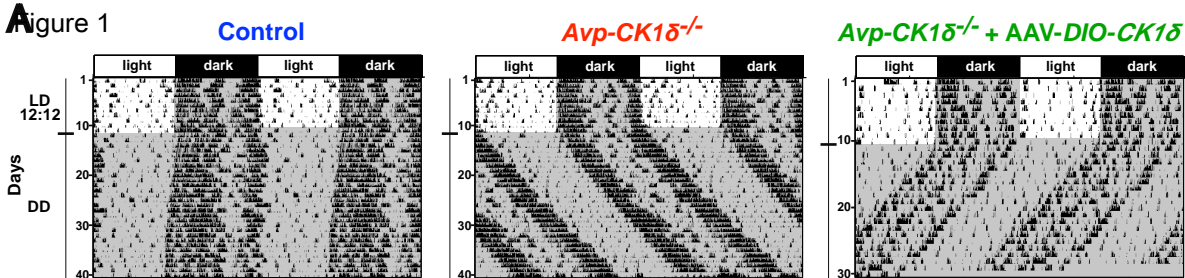
REFERENCES

1. Welsh, D.K., Takahashi, J.S., and Kay, S.A. (2010). Suprachiasmatic nucleus: cell autonomy and network properties. *Annu Rev Physiol* 72, 551-577.
2. Antle, M.C., and Silver, R. (2005). Orchestrating time: arrangements of the brain circadian clock. *Trends Neurosci* 28, 145-151.
3. Etchegaray, J.P., Machida, K.K., Noton, E., Constance, C.M., Dallmann, R., Di Napoli, M.N., DeBruyne, J.P., Lambert, C.M., Yu, E.A., Reppert, S.M., et al. (2009). Casein kinase 1 delta regulates the pace of the mammalian circadian clock. *Mol Cell Biol* 29, 3853-3866.
4. Etchegaray, J.P., Yu, E.A., Indic, P., Dallmann, R., and Weaver, D.R. (2010). Casein kinase 1 delta (CK1delta) regulates period length of the mouse suprachiasmatic circadian clock in vitro. *PLoS One* 5, e10303.
5. Lee, H., Chen, R., Lee, Y., Yoo, S., and Lee, C. (2009). Essential roles of CK1delta and CK1epsilon in the mammalian circadian clock. *Proc Natl Acad Sci U S A* 106, 21359-21364.
6. Tsuchiya, Y., Umemura, Y., Minami, Y., Koike, N., Hosokawa, T., Hara, M., Ito, H., Inokawa, H., and Yagita, K. (2016). Effect of Multiple Clock Gene Ablations on the Circadian Period Length and Temperature Compensation in Mammalian Cells. *J Biol Rhythms* 31, 48-56.
7. Akashi, M., Tsuchiya, Y., Yoshino, T., and Nishida, E. (2002). Control of intracellular dynamics of mammalian period proteins by casein kinase I epsilon (CK1epsilon) and CK1delta in cultured cells. *Mol Cell Biol* 22, 1693-1703.
8. Camacho, F., Cilio, M., Guo, Y., Virshup, D.M., Patel, K., Khorkova, O., Styren, S., Morse, B., Yao, Z., and Keesler, G.A. (2001). Human casein kinase Idelta phosphorylation of human circadian clock proteins period 1 and 2. *FEBS Lett* 489, 159-165.
9. Isojima, Y., Nakajima, M., Ukai, H., Fujishima, H., Yamada, R.G., Masumoto, K.H., Kiuchi, R., Ishida, M., Ukai-Tadenuma, M., Minami, Y., et al. (2009). CK1epsilon/delta-dependent phosphorylation is a temperature-insensitive,

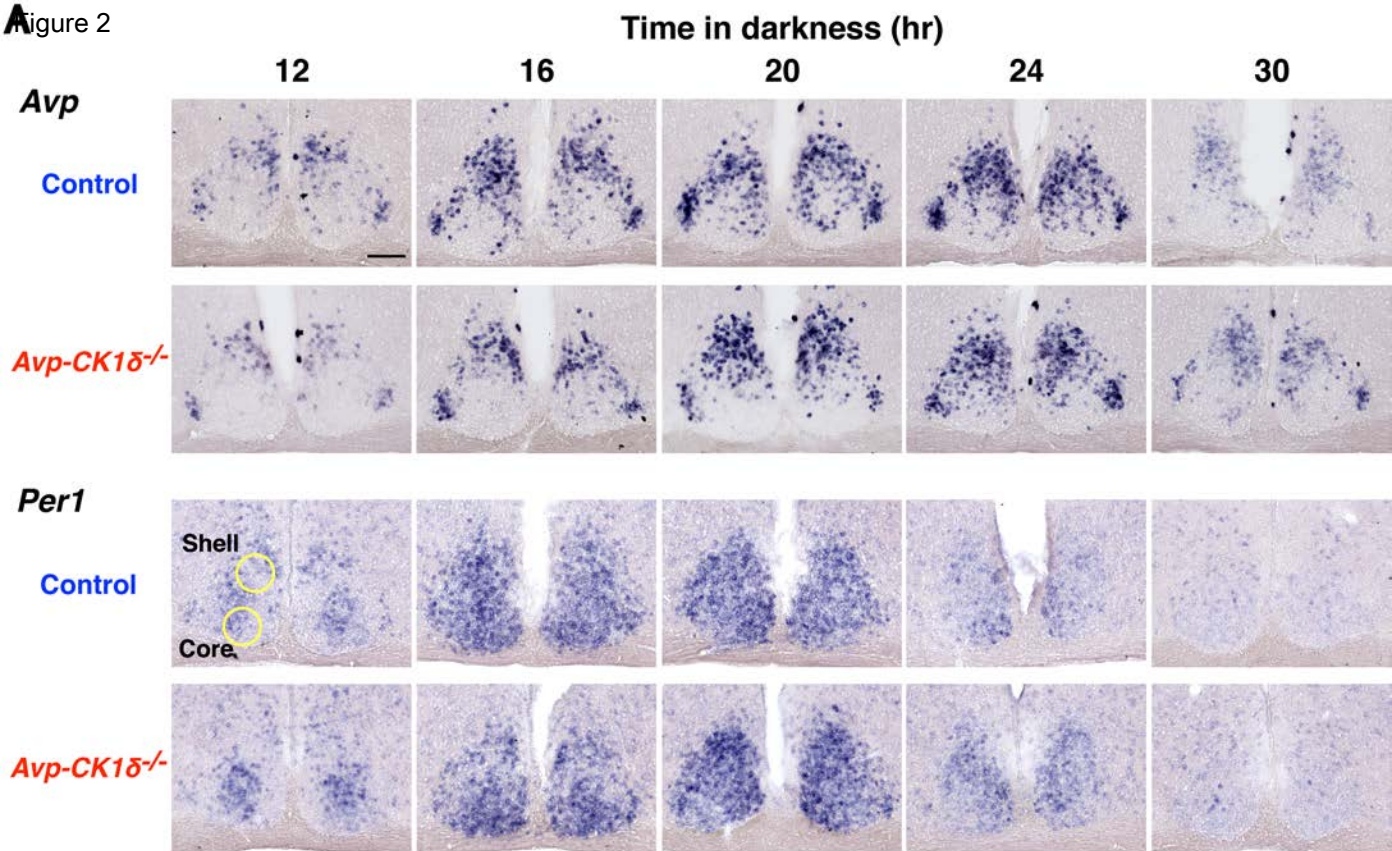
- period-determining process in the mammalian circadian clock. *Proc Natl Acad Sci U S A* 106, 15744-15749.
10. Meng, Q.J., Maywood, E.S., Bechtold, D.A., Lu, W.Q., Li, J., Gibbs, J.E., Dupre, S.M., Chesham, J.E., Rajamohan, F., Knafels, J., et al. (2010). Entrainment of disrupted circadian behavior through inhibition of casein kinase 1 (CK1) enzymes. *Proc Natl Acad Sci U S A* 107, 15240-15245.
 11. Xu, Y., Padiath, Q.S., Shapiro, R.E., Jones, C.R., Wu, S.C., Saigoh, N., Saigoh, K., Ptacek, L.J., and Fu, Y.H. (2005). Functional consequences of a CK1delta mutation causing familial advanced sleep phase syndrome. *Nature* 434, 640-644.
 12. Xu, Y., Toh, K.L., Jones, C.R., Shin, J.Y., Fu, Y.H., and Ptacek, L.J. (2007). Modeling of a human circadian mutation yields insights into clock regulation by PER2. *Cell* 128, 59-70.
 13. Zhou, M., Kim, J.K., Eng, G.W., Forger, D.B., and Virshup, D.M. (2015). A Period2 Phosphoswitch Regulates and Temperature Compensates Circadian Period. *Mol Cell* 60, 77-88.
 14. Mieda, M., Ono, D., Hasegawa, E., Okamoto, H., Honma, K., Honma, S., and Sakurai, T. (2015). Cellular clocks in AVP neurons of the SCN are critical for interneuronal coupling regulating circadian behavior rhythm. *Neuron* 85, 1103-1116.
 15. Aschoff, J., Hoffmann, K., Pohl, H., and Wever, R. (1975). Re-entrainment of circadian rhythms after phase-shifts of the Zeitgeber. *Chronobiologia* 2, 23-78.
 16. Pittendrigh, C.S., and Daan, S. (1976). A functional analysis of circadian pacemakers in nocturnal rodents. IV. Entrainment: Pacemaker as clock. *J Comp Physiol* 106, 291-331.
 17. Yoo, S.H., Yamazaki, S., Lowrey, P.L., Shimomura, K., Ko, C.H., Buhr, E.D., Siepk, S.M., Hong, H.K., Oh, W.J., Yoo, O.J., et al. (2004). PERIOD2::LUCIFERASE real-time reporting of circadian dynamics reveals persistent circadian oscillations in mouse peripheral tissues. *Proc Natl Acad Sci U S A* 101, 5339-5346.

18. Smyllie, N.J., Chesham, J.E., Hamnett, R., Maywood, E.S., and Hastings, M.H. (2016). Temporally chimeric mice reveal flexibility of circadian period-setting in the suprachiasmatic nucleus. *Proc Natl Acad Sci U S A* 113, 3657-3662.
19. Yamaguchi, S., Isejima, H., Matsuo, T., Okura, R., Yagita, K., Kobayashi, M., and Okamura, H. (2003). Synchronization of cellular clocks in the suprachiasmatic nucleus. *Science* 302, 1408-1412.
20. Enoki, R., Kuroda, S., Ono, D., Hasan, M.T., Ueda, T., Honma, S., and Honma, K. (2012). Topological specificity and hierarchical network of the circadian calcium rhythm in the suprachiasmatic nucleus. *Proc Natl Acad Sci U S A* 109, 21498-21503.
21. Kalsbeek, A., Fliers, E., Hofman, M.A., Swaab, D.F., and Buijs, R.M. (2010). Vasopressin and the output of the hypothalamic biological clock. *J Neuroendocrinol* 22, 362-372.
22. Yamaguchi, Y., Suzuki, T., Mizoro, Y., Kori, H., Okada, K., Chen, Y., Fustin, J.M., Yamazaki, F., Mizuguchi, N., Zhang, J., et al. (2013). Mice genetically deficient in vasopressin V1a and V1b receptors are resistant to jet lag. *Science* 342, 85-90.
23. Low-Zeddies, S.S., and Takahashi, J.S. (2001). Chimera analysis of the Clock mutation in mice shows that complex cellular integration determines circadian behavior. *Cell* 105, 25-42.
24. Lee, I.T., Chang, A.S., Manandhar, M., Shan, Y., Fan, J., Izumo, M., Ikeda, Y., Motoike, T., Dixon, S., Seinfeld, J.E., et al. (2015). Neuromedin s-producing neurons act as essential pacemakers in the suprachiasmatic nucleus to couple clock neurons and dictate circadian rhythms. *Neuron* 85, 1086-1102.
25. Aton, S.J., Colwell, C.S., Harmor, A.J., Waschek, J., and Herzog, E.D. (2005). Vasoactive intestinal polypeptide mediates circadian rhythmicity and synchrony in mammalian clock neurons. *Nat Neurosci* 8, 476-483.
26. Colwell, C.S., Michel, S., Itri, J., Rodriguez, W., Tam, J., Lelievre, V., Hu, Z., Liu, X., and Waschek, J.A. (2003). Disrupted circadian rhythms in VIP- and PHI-deficient mice. *Am J Physiol Regul Integr Comp Physiol* 285, R939-949.

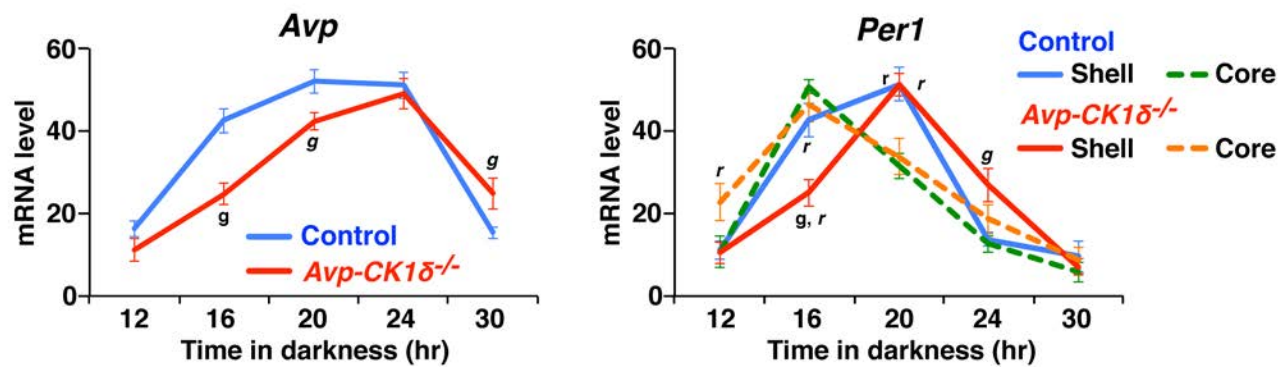
27. Harmar, A.J., Marston, H.M., Shen, S., Spratt, C., West, K.M., Sheward, W.J., Morrison, C.F., Dorin, J.R., Piggins, H.D., Reubi, J.C., et al. (2002). The VPAC(2) receptor is essential for circadian function in the mouse suprachiasmatic nuclei. *Cell* 109, 497-508.
28. Maywood, E.S., Reddy, A.B., Wong, G.K., O'Neill, J.S., O'Brien, J.A., McMahon, D.G., Harmar, A.J., Okamura, H., and Hastings, M.H. (2006). Synchronization and maintenance of timekeeping in suprachiasmatic circadian clock cells by neuropeptidergic signaling. *Curr Biol* 16, 599-605.
29. Ko, C.H., Yamada, Y.R., Welsh, D.K., Buhr, E.D., Liu, A.C., Zhang, E.E., Ralph, M.R., Kay, S.A., Forger, D.B., and Takahashi, J.S. (2010). Emergence of noise-induced oscillations in the central circadian pacemaker. *PLoS Biol* 8, e1000513.
30. Baba, K., Ono, D., Honma, S., and Honma, K. (2008). A TTX-sensitive local circuit is involved in the expression of PK2 and BDNF circadian rhythms in the mouse suprachiasmatic nucleus. *Eur J Neurosci* 27, 909-916.
31. Ono, D., Honma, S., and Honma, K. (2013). Cryptochromes are critical for the development of coherent circadian rhythms in the mouse suprachiasmatic nucleus. *Nat Commun* 4, 1666.
32. Pennartz, C.M., de Jeu, M.T., Bos, N.P., Schaap, J., and Geurtsen, A.M. (2002). Diurnal modulation of pacemaker potentials and calcium current in the mammalian circadian clock. *Nature* 416, 286-290.
33. Inagaki, N., Honma, S., Ono, D., Tanahashi, Y., and Honma, K. (2007). Separate oscillating cell groups in mouse suprachiasmatic nucleus couple photoperiodically to the onset and end of daily activity. *Proc Natl Acad Sci U S A* 104, 7664-7669.



A Figure 2



B



A Figure 3

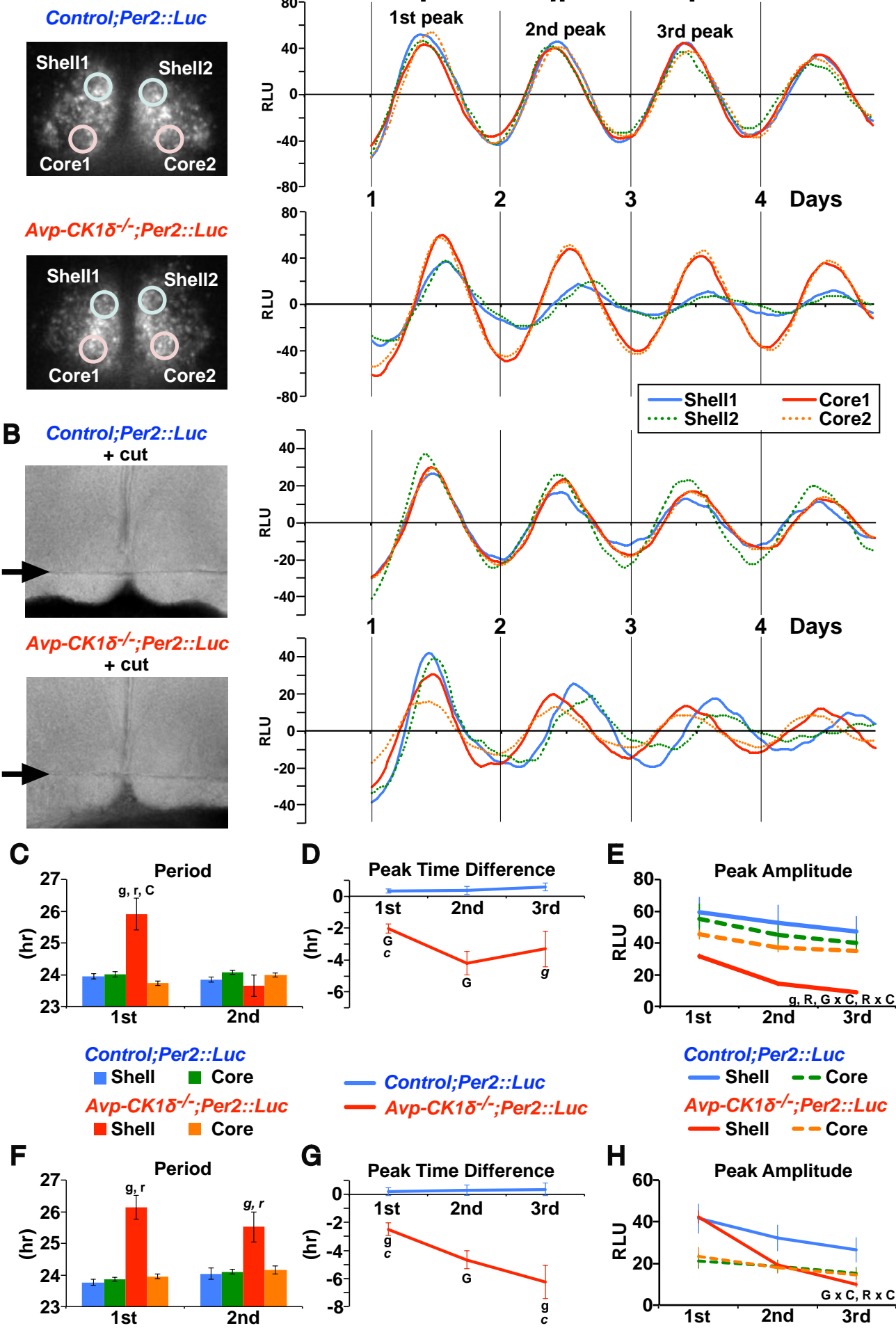
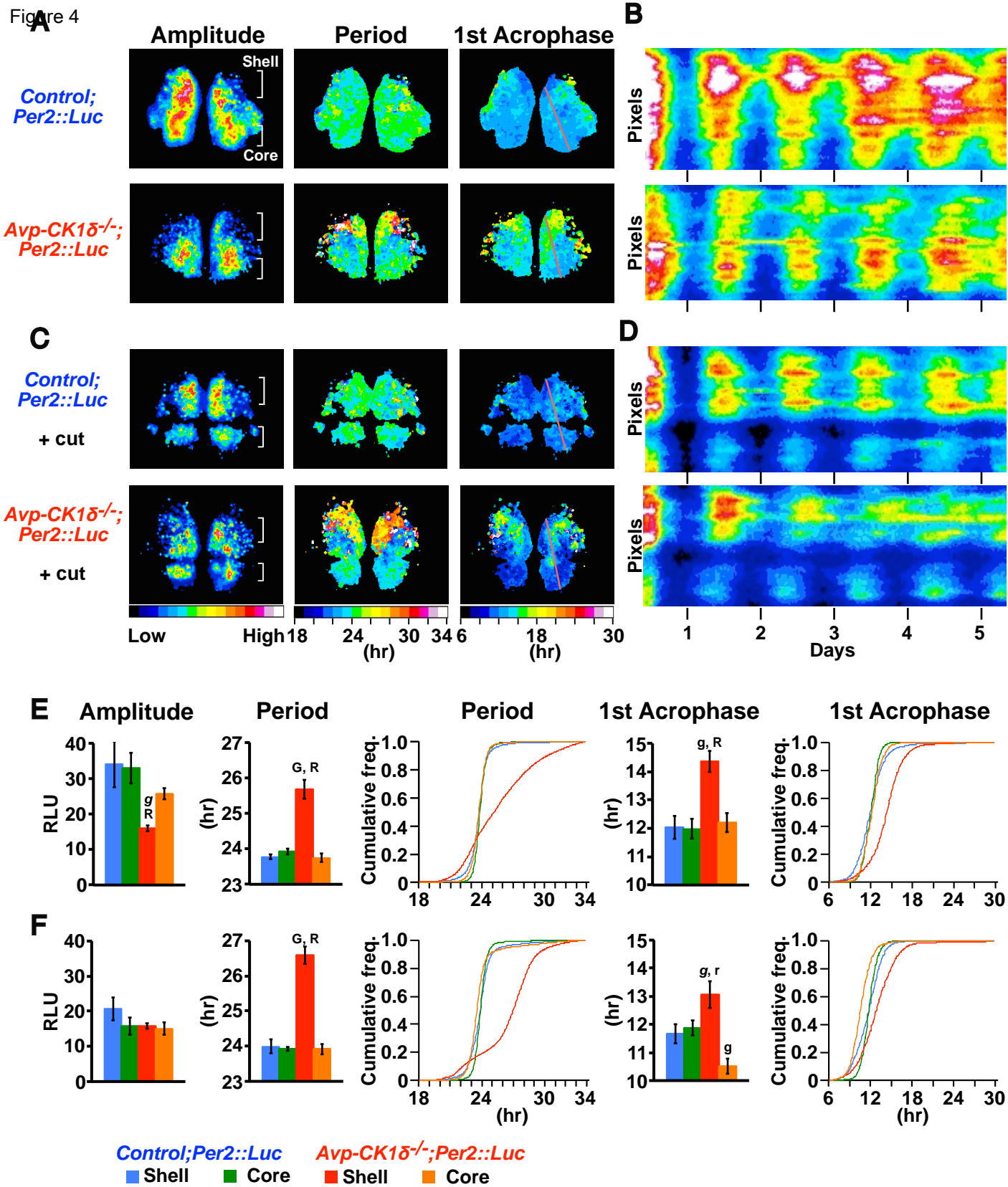


Figure 4



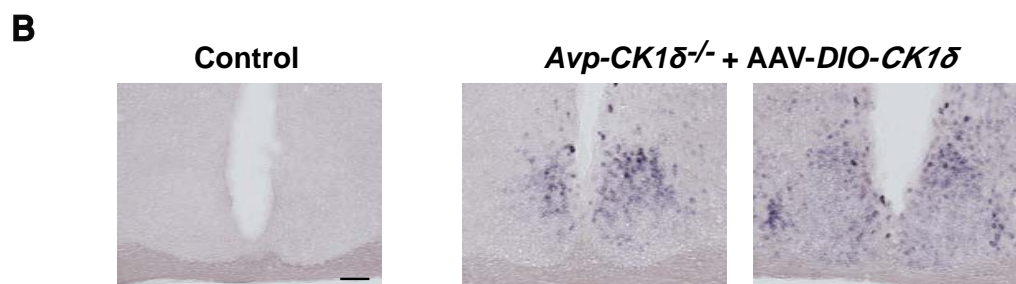
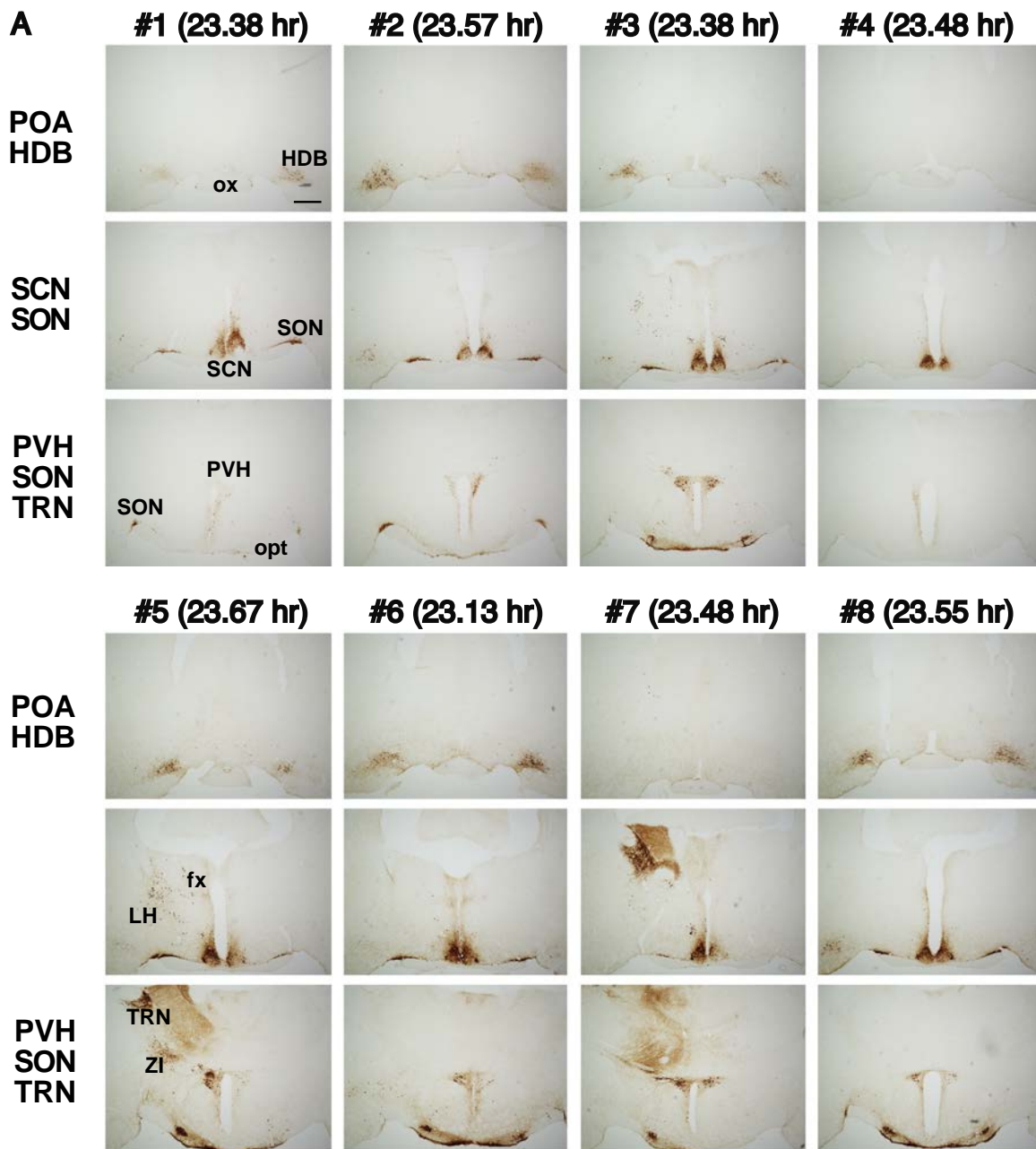


Figure S1. Distributions of *CK1δ*-overexpressing cells in *Avp-CK1δ^{-/-}+AAV-DIO-CK1δ* mice, related to Figure 1. Mixture of recombinant AAV vectors expressing *CK1δ* or *mCherry* in a Cre-dependent manner by means of DIO (double-floxed inverse open reading frame)/FLEX (flip-excision) switch was focally injected into the SCN. The ratio of *AAV-DIO-CK1δ* to *AAV-DIO-mCherry* was 5:1. (A) Representative images of slices prepared from 8 individual *Avp-CK1δ^{-/-}+AAV-DIO-CK1δ* mice and stained with anti-DsRed antibody to detect mCherry expression are shown. The free-running period of each mouse is indicated in parentheses. In addition to the SCN, some off-target expression was observed in a small number of scattered neuronal cell bodies and fibers in the supraoptic nucleus (SON), paraventricular hypothalamic nucleus (PVH), and nucleus of the horizontal limb of the diagonal band (HDB) of most mice as well as in the thalamic reticular nucleus (TRN) and zona incerta (ZI) of a few mice. Note that mCherry+ cells were almost completely restricted to the SCN in mouse #4 whose free-running period was still shorter (23.48 hr) as compared to those of control mice. (B) Representative images of *CK1δ* mRNA expression in the SCN of control (*Avp-CK1δ^{-/-}+AAV-DIO-mCherry*) and *Avp-CK1δ^{-/-}+AAV-DIO-CK1δ* mice. Coronal sections were hybridized in situ to an antisense probe for *CK1δ*. Under the condition used in the current study, *CK1δ* mRNA expression was lower than the detection limit in control mice, while it was clearly observed in the shell of the SCN in *Avp-CK1δ^{-/-}+AAV-DIO-CK1δ* mice.

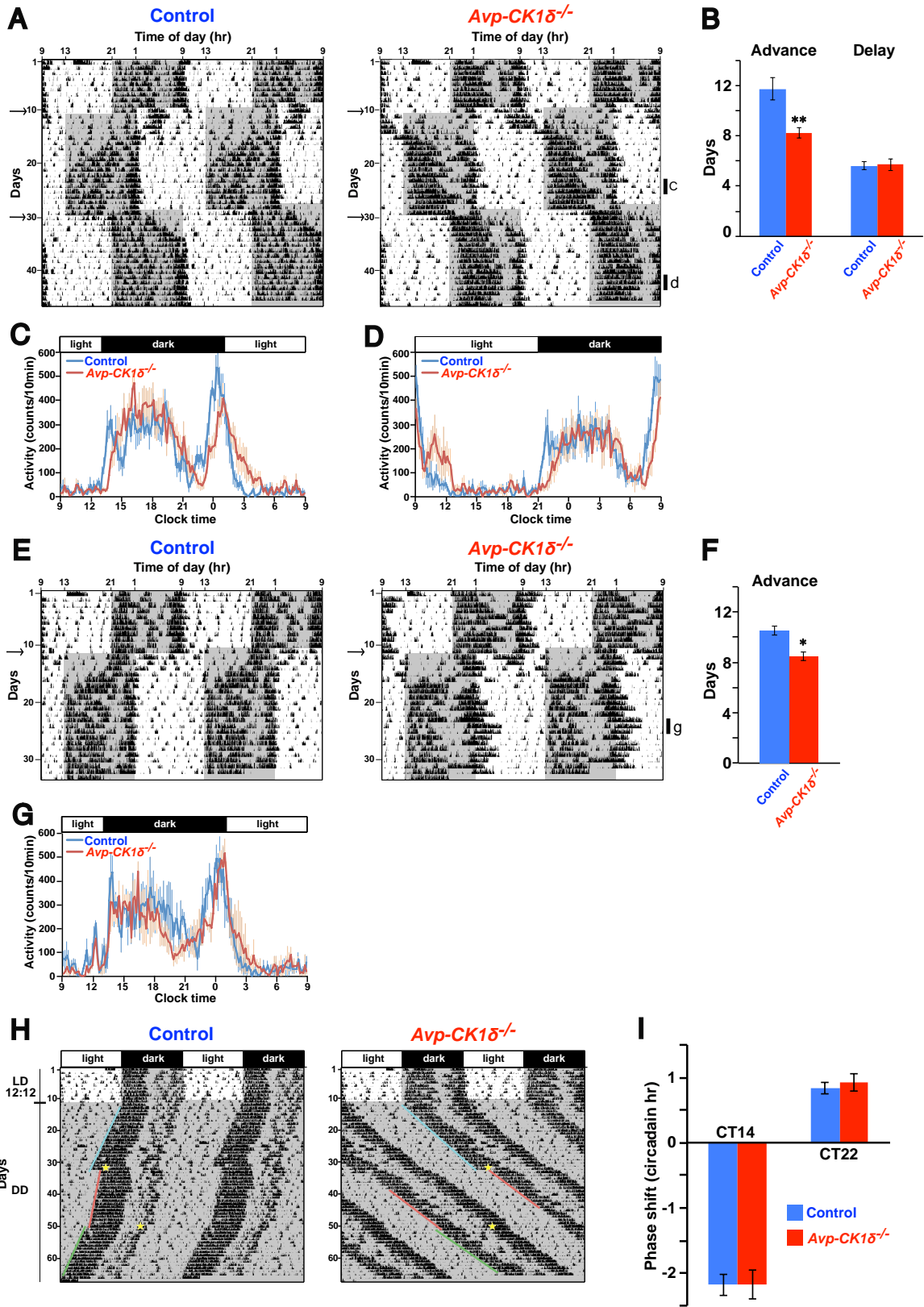


Figure S2. *Avp-CK1 δ ^{-/-}* mice reentrain to the 8-hr phase advance of LD cycle by delaying their behavior rhythm, related to Figure 1. (A) Representative locomotor activity of control and *Avp-CK1 δ ^{-/-}* mice. All control mice (8 of 8) advanced their activity rhythm, while all *Avp-CK1 δ ^{-/-}* mice (7 of 7) delayed, upon 8-hr phase advance of LD cycle. (B) The number of days required for reentrainment to the 8-hr phase advance was reduced in *Avp-CK1 δ ^{-/-}* mice. Error bars indicate S.E.M. **, $p < 0.01$. (C, D) Daily profiles of locomotor activity during the days indicated by vertical bars on the right side of the actogram. The phase angle of entrainment in *Avp-CK1 δ ^{-/-}* mice was delayed in new LD cycles. (E) LD cycle was phase-advanced for 8 hr in a way different from (A): the light phase was shortened at the beginning of phase shift (day 11, indicated by arrows). Although as unclear as in (A), all *Avp-CK1 δ ^{-/-}* mice (4 of 4) delayed their activity rhythm with an 8-hr phase advance. (F) The number of days required for reentrainment to the 8-hr phase advance in (E) was reduced in *Avp-CK1 δ ^{-/-}* mice. *, $p < 0.05$. (G) Daily profiles of locomotor activity during the days indicated by vertical bars on the right side of the actogram in (E). In this experiment, significant delay of the phase angle of entrainment was not observed in *Avp-CK1 δ ^{-/-}* mice. (H) Phase-shifting responses to light are unchanged in *Avp-CK1 δ ^{-/-}* mice. Representative locomotor activity of control and *Avp-CK1 δ ^{-/-}* mice are shown. Mice were given a 30 min light pulse at CT14 or CT22 as indicated by yellow stars on actograms. (I) Phase shifts induced by a 30-min light pulse at ZT14 or ZT22; $n = 6$.

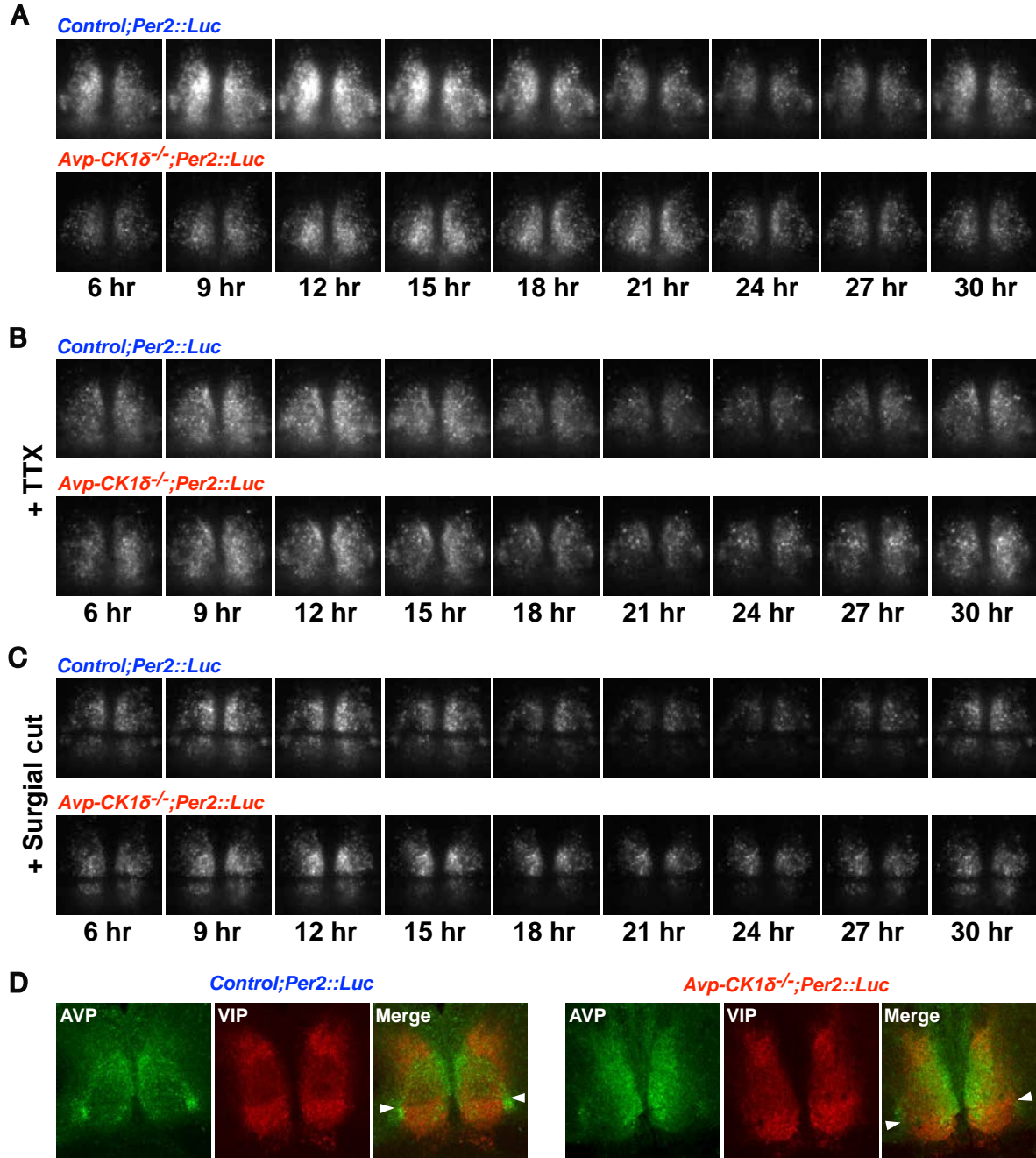


Figure S3. Spatiotemporal pattern of PER2::LUC oscillation is altered in the SCN of *Avp-CK1 δ ^{-/-}* mice, related to Figure 3. (A-C) Representative bioluminescence recording from intact (A), TTX-treated (B), or surgically cut (C) SCN slices. “6 hr” corresponds to the first CT6 after slice preparation, determined according to behavioral free-running period before slice preparation. (D) SCN explants with surgical cuts were double-immunostained for AVP (green) and VIP (red). The locations of surgical cuts are indicated by arrowheads.

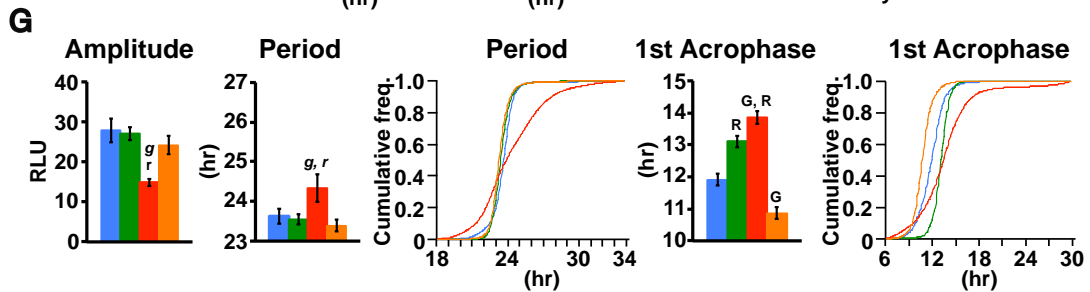
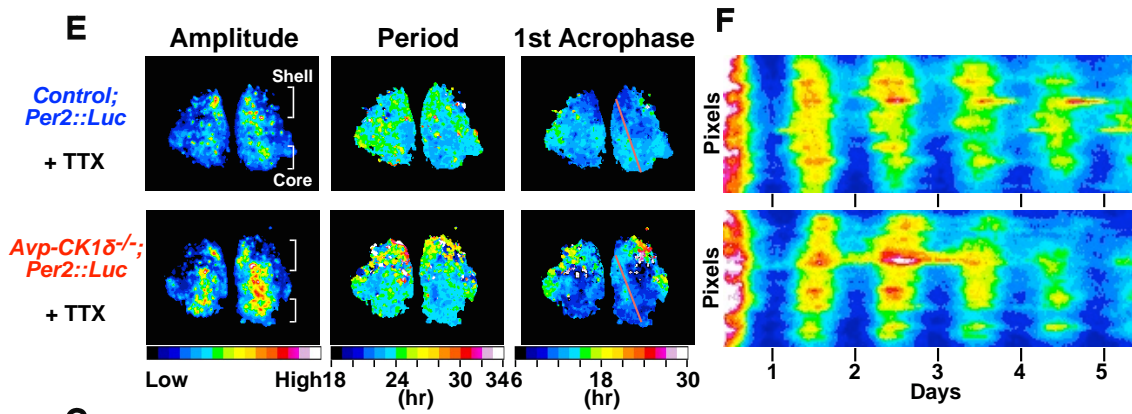
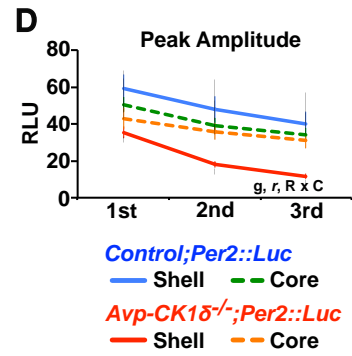
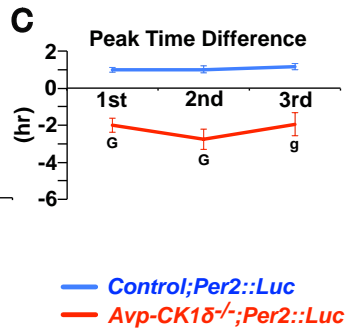
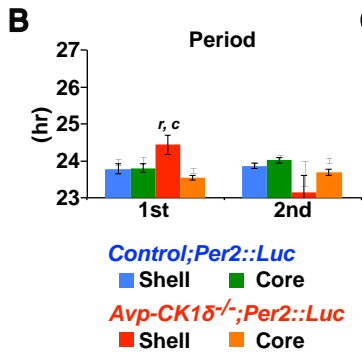
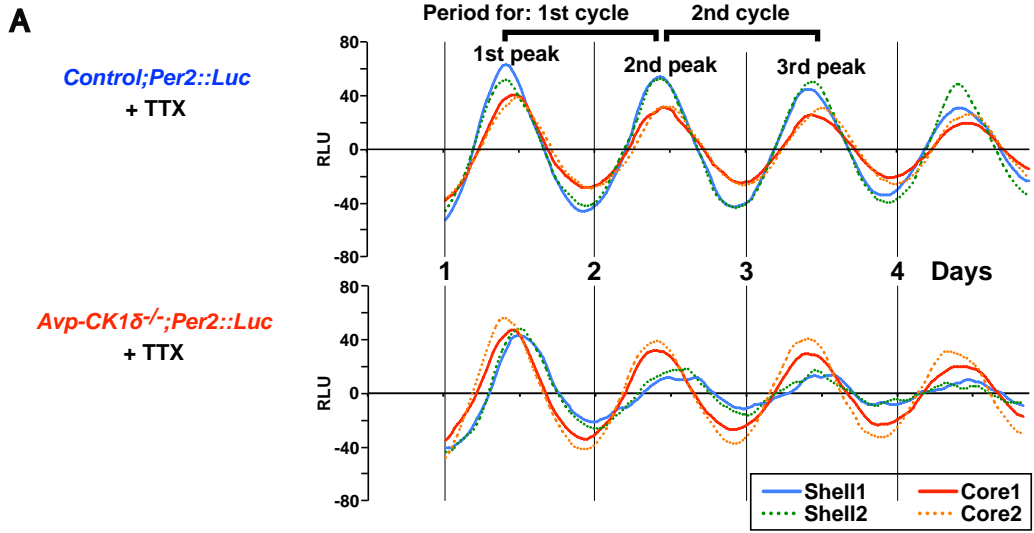


Figure S4. Effect of TTX on PER2::LUC oscillation, related to Figures 3 and 4. (A) Coronal SCN slices of the mid-rostrocaudal region were cultured with 2.5 μ M TTX. Detrended bioluminescence within the two shell and two core regions as indicated in Figure 3A were plotted. Gray vertical lines labeled “Day 1” indicate 15 hr after the start of image recordings around CT9. (B) Period of PER2::LUC oscillations for two cycles defined in (A). (C) Peak time differences between the shell and core of the SCN. (D) Amplitudes of the three peaks defined in (A). Error bars indicate S.E.M; n = 5 for control, n = 6 for *Avp-CK1 δ ^{-/-};Per2::Luc* mice. 1 μ M TTX was applied for two control and three *Avp-CK1 δ ^{-/-}* slices, while 2.5 μ M TTX was applied for the rest. Because the effects of two concentrations were similar, we processed two groups together. For (B, C), G, effect of genotype in each region for each cycle; R, effect of region in each genotype for each cycle; C, effect of cycle in each region of each genotype; by post hoc pairwise comparisons. For (D), G, effect of genotype in the shell; R, effect of region in *Avp-CK1 δ ^{-/-}* mice; R x C, interaction between region and cycle in *Avp-CK1 δ ^{-/-}* mice; by two-way repeated-measures ANOVA; uppercase, p < 0.001; lowercase, p < 0.01; italicized lowercase, p < 0.05. (E) Representative amplitude, period, and first acrophase maps of PER2::LUC oscillation at the pixel level of TTX-treated SCN slices. Amplitudes, periods, and acrophases of PER2::LUC oscillations in the individual pixels covering the SCN were calculated by cosine curve fittings for data representing 72 hr from the first CT6 after slice preparation, determined according to behavioral free-running period before slice preparation. For the first acrophase, “6 hr” corresponds to the beginning of cosine curved-fitted data at roughly CT6. (F) Raster plots of signal intensity from the dorsal tip to the end of ventral region as indicated by red lines in (E). (G) Mean and cumulative frequency of period and first acrophase of individual pixels’ PER2::LUC oscillations. The dorsal 40% and ventral 30% regions of the SCN were regarded as the shell and core, respectively. Representative regions defined as the SCN shell or core are indicated in (E). n = 5 for control, n = 6 for *Avp-CK1 δ ^{-/-};Per2::Luc* mice. G, effect of genotype in each region; R, effect of region in each genotype; by post hoc pairwise comparisons; uppercase, p < 0.001; lowercase, p < 0.01; italicized lowercase, p < 0.05.

Table S1. Comparison of two genotypes regarded as control		
Genotype	<i>CK1δ^{flox2/flox2}</i>	<i>Avp-Cre;CK1δ^{S+/flox2}</i>
<i>n</i>	10	4
Light-Dark (7 days)		
Amplitude (Qp)	3466.14 ± 195.78	3924.64 ± 437.24
Activity time (hr)	12.49 ± 0.16	12.76 ± 0.16
Activity onset (ZT)	12.09 ± 0.02	12.01 ± 0.03
Activity offset (ZT)	0.59 ± 0.15	0.77 ± 0.14
Activity (count)		
Dark period	16427 ± 1099	20247 ± 5198
Light period	3365 ± 207	3538 ± 576
24 hr	19792 ± 1182	23785 ± 5771
Constant Darkness (days 5-19)		
Amplitude (Qp)	6377.61 ± 347.14	5942.62 ± 499.40
Free-running period (hr)		
Periodogram	23.92 ± 0.03	24.00 ± 0.04
Visual inspection		
Activity onset	23.89 ± 0.03	23.99 ± 0.04
Activity offset	23.93 ± 0.03	24.00 ± 0.06
Activity time (circadian hr)		
Activity profile	13.30 ± 0.25	13.73 ± 0.39
Visual inspection	13.09 ± 0.25	13.76 ± 0.32
Cycle-to-cycle variability (SD) (min) – Visual inspection		
Activity onset	13.98 ± 0.68	14.70 ± 1.26
Activity offset	37.14 ± 3.75	34.05 ± 3.27
Activity (count)		
Activity period	18602 ± 1009	21000 ± 3880
Rest period	2670 ± 239	2394 ± 641
Free-running period	21302 ± 1147	23394 ± 4488

Table S1. Comparison of two genotypes regarded as control. Significant differences between *CK1δ^{flox2/flox2}* and *Avp-Cre;CK1δ^{S+/flox2}* mice were not detected in any parameters by Student's t tests.

Table S2. Phenotypic Characteristics of <i>Avp-CK1δ^{-/-}</i> Mice				
Genotype	Control	<i>Avp-CK1δ^{-/-}</i>	<i>Avp-CK1δ^{-/-}</i> + AAV- <i>DIO-CK1δ</i>	<i>Avp-CK1δ^{-/-}</i> + AAV- <i>DIO-mCherry</i>
<i>n</i>	14	13	8	6
Light-Dark (7 days)				
Amplitude (Qp)	3597.14 ± 186.71	3847.11 ± 158.63	3346.14 ± 230.33	3685.99 ± 182.44
Activity time (hr)	12.57 ± 0.12	12.76 ± 0.19	12.19 ± 0.18	11.99 ± 0.07**^^
Activity onset (ZT)	12.07 ± 0.02	12.32 ± 0.10	12.03 ± 0.09	12.49 ± 0.15
Activity offset (ZT)	0.64 ± 0.12	1.07 ± 0.19	0.22 ± 0.20^	0.48 ± 0.13
Activity (count)				
Dark period	17519 ± 1615	16028 ± 1168	14473 ± 896	15274 ± 1809
Light period	3414 ± 209	4565 ± 427	2622 ± 450^	2924 ± 499^
24 hr	20933 ± 1771	20594 ± 1360	17095 ± 1237	18199 ± 1657
Constant Darkness (days 5-19)				
Amplitude (Qp)	6253.33 ± 281.08	7366.32 ± 395.38	5311.47 ± 537.70	5644.51 ± 409.46
Free-running period (hr)				
Periodogram	23.94 ± 0.03	24.72 ± 0.03***	23.46 ± 0.06***^^^	24.52 ± 0.04**^#
Visual inspection				
Activity onset	23.91 ± 0.03	24.70 ± 0.03***	23.39 ± 0.05***^^^	24.50 ± 0.04**^#
Activity offset	23.95 ± 0.03	24.78 ± 0.02***	23.46 ± 0.06***^^^	24.56 ± 0.04**^#
Activity time (circadian hr)				
Activity profile	13.42 ± 0.21	13.96 ± 0.19	13.73 ± 0.30	12.73 ± 0.22^
Visual inspection	13.32 ± 0.21	13.94 ± 0.19**	13.00 ± 0.37^	12.90 ± 0.19^
Cycle-to-cycle variability (SD) (min) – Visual inspection				
Activity onset	14.19 ± 0.58	20.49 ± 2.21*	21.68 ± 2.22*	16.70 ± 2.64
Activity offset	36.26 ± 2.79	30.37 ± 2.55	30.08 ± 3.93	24.50 ± 2.64
Activity (count)				
Activity period	19287 ± 1260	22145 ± 1189	13580 ± 706***^^	13988 ± 1060***^^
Rest period	2612 ± 238	2149 ± 192	1644 ± 211*	1830 ± 347*
Total	21900 ± 1431	24294 ± 1287	15224 ± 831***^^	15818 ± 1236***^^

Table S2. Phenotypic characterization of *Avp-CK1δ^{-/-}* mice, related to Figure 1. Control includes *CK1δ^{flox2/flox2}* and *Avp-Cre;CK1δ^{+flox2}* mice. Values are mean ± S.E.M. For comparison between control, *Avp-CK1δ^{-/-}*, *Avp-CK1δ^{-/-}*+AAV-*DIO-CK1δ*, and *Avp-CK1δ^{-/-}*+AAV-*DIO-mCherry* (control for AAV injection) mice, effects of genotype were analyzed by Kruskal-Wallis tests followed by Steel-Dwass post hoc tests. *, versus control mice; ^, versus *Avp-CK1δ^{-/-}* mice; #, versus *Avp-CK1δ^{-/-}*+AAV-*DIO-CK1δ* mice; one letter, p < 0.05; two letters, p < 0.01; three letters, p < 0.001.

Table S3. Summary of PER2::LUC imaging studies (ROI analysis)

No treatment				
Genotype	Control		<i>Avp-CK1δ^{-/-}</i>	
<i>n</i>	5		7	
Region	Shell	Core	Shell	Core
Period (hr)				
1st cycle	23.95 ± 0.08	24.00 ± 0.08	25.91 ± 0.50 ^{g, r, c}	23.72 ± 0.07
2nd cycle	23.85 ± 0.08	24.07 ± 0.06	23.65 ± 0.33	23.98 ± 0.06
Peak time difference (hr)				
1st peak	0.32 ± 0.13		-2.02 ± 0.29 ^{G, c}	
2nd peak	0.37 ± 0.26		-4.21 ± 0.74 ^G	
3rd peak	0.59 ± 0.26		-3.31 ± 1.12 ^g	
Peak amplitude (RLU)				
1st peak	59.28 ± 9.91 ^c	55.34 ± 9.36 ^c	31.57 ± 1.69 ^{g, r, c}	45.42 ± 3.19 ^c
2nd peak	52.82 ± 10.98	44.87 ± 7.74	14.27 ± 1.48 ^{g, R}	36.87 ± 2.89
3rd peak	47.20 ± 9.64 ^c	39.86 ± 6.27	9.10 ± 1.40 ^{g, R, c}	34.83 ± 2.90
+ TTX				
Genotype	Control		<i>Avp-CK1δ^{-/-}</i>	
<i>n</i>	5		6	
Region	Shell	Core	Shell	Core
Period (hr)				
1st cycle	23.78 ± 0.14	23.81 ± 0.12	24.44 ± 0.27 ^{r, c}	23.55 ± 0.07
2nd cycle	23.87 ± 0.08	24.02 ± 0.08	23.15 ± 0.46	23.69 ± 0.08
Peak time difference (hr)				
1st peak	0.98 ± 0.13		-1.99 ± 0.39 ^G	
2nd peak	1.00 ± 0.20		-2.76 ± 0.55 ^G	
3rd peak	1.15 ± 0.17		-1.95 ± 0.62 ^g	
Peak amplitude (RLU)				
1st peak	59.26 ± 7.72 ^c	50.73 ± 4.03 ^c	35.55 ± 3.24 ^{g, c}	43.08 ± 5.80 ^c
2nd peak	47.89 ± 7.14	39.08 ± 4.23	18.03 ± 1.74 ^{g, r}	35.97 ± 4.56
3rd peak	40.10 ± 6.44 ^c	34.18 ± 3.54 ^c	11.55 ± 1.30 ^{g, r, c}	30.96 ± 4.10 ^c
+ Surgical cut				
Genotype	Control		<i>Avp-CK1δ^{-/-}</i>	
<i>n</i>	5		5	
Region	Shell	Core	Shell	Core
Period (hr)				
1st cycle	23.77 ± 0.10	23.86 ± 0.07	26.14 ± 0.38 ^{g, r}	23.96 ± 0.08
2nd cycle	24.04 ± 0.17	24.10 ± 0.08	25.52 ± 0.48 ^{g, r}	24.15 ± 0.13
Peak time difference (hr)				
1st peak	0.20 ± 0.29		-2.48 ± 0.47 ^{g, c}	
2nd peak	0.29 ± 0.36		-4.67 ± 0.64 ^G	
3rd peak	0.35 ± 0.46		-6.26 ± 1.18 ^{g, c}	
Peak amplitude (RLU)				
1st peak	41.53 ± 7.12 ^{r, c}	21.11 ± 3.59 ^c	42.34 ± 3.13 ^{r, c}	23.36 ± 4.28
2nd peak	32.18 ± 6.39	18.71 ± 3.12	19.30 ± 1.67	18.14 ± 2.91
3rd peak	26.54 ± 5.93 ^c	15.29 ± 2.87 ^c	9.94 ± 1.56 ^{g, c}	14.48 ± 2.65 ^c

Table S3. Summary of PER2::LUC imaging studies (ROI analysis), related to Figure 3. Values are mean \pm S.E.M. Two-way repeated-measures ANOVA was followed by post hoc tests as below. To compare the two groups, Student's t tests or paired t tests were performed; Welch's t test was used when the variances of the two groups differed significantly. To compare the three groups, Friedman tests followed by Wilcoxon signed-rank tests were performed. G, effect of genotype in each region for each cycle; R, effect of region in each genotype for each cycle; C, effect of cycle (versus 2nd) in each region of each genotype; by post-hoc pairwise comparisons; uppercase, $p < 0.001$; lowercase, $p < 0.01$; italicized lowercase, $p < 0.05$.

Table S4. Summary of PER2::LUC imaging studies (cosine curve fitting)				
<u>No treatment</u>				
Genotype	Control		<i>Avp-CK1δ^{-/-}</i>	
<i>n</i>	5		7	
Region	Shell	Core	Shell	Core
Amplitude (RLU)	34.05 ± 6.49	32.92 ± 4.25	15.94 ± 0.79 ^{g, R}	25.72 ± 1.52
Period (hr)	23.78 ± 0.07	23.92 ± 0.07	25.68 ± 0.27 ^{G, R}	23.75 ± 0.11
1st acrophase (hr)	6.03 ± 0.40	5.98 ± 0.34	8.35 ± 0.37 ^{g, R}	6.20 ± 0.34
<u>+ TTX</u>				
Genotype	Control		<i>Avp-CK1δ^{-/-}</i>	
<i>n</i>	5		6	
Region	Shell	Core	Shell	Core
Amplitude (RLU)	27.81 ± 3.00	27.05 ± 1.60	14.85 ± 0.88 ^{g, r}	24.13 ± 2.31
Period (hr)	23.63 ± 0.19	23.56 ± 0.13	24.33 ± 0.34 ^g	23.39 ± 0.15
1st acrophase (hr)	5.91 ± 0.19	7.11 ± 0.19 ^R	7.86 ± 0.20 ^{G, R}	4.87 ± 0.19 ^G
<u>+ Surgical cut</u>				
Genotype	Control		<i>Avp-CK1δ^{-/-}</i>	
<i>n</i>	5		5	
Region	Shell	Core	Shell	Core
Amplitude (RLU)	20.65 ± 3.36	15.76 ± 2.44	15.80 ± 0.74	15.09 ± 1.86
Period (hr)	23.99 ± 0.19	23.93 ± 0.06	26.59 ± 0.25 ^{G, R}	23.92 ± 0.15
1st acrophase (hr)	5.66 ± 0.34	5.87 ± 0.26	7.05 ± 0.48 ^{g, r}	4.51 ± 0.27 ^g

Table S4. Summary of PER2::LUC imaging studies (pixel-based analysis), related to Figure 4. Values are mean ± S.E.M. Two-way repeated-measures ANOVA followed by post hoc Student's t tests or paired t tests were performed; Welch's t test was used when the variances of the two groups differed significantly. G, effect of genotype in each region; R, effect of region in each genotype; by post-hoc pairwise comparisons; uppercase, p < 0.001; lowercase, p < 0.01; italicized lowercase, p < 0.05.

SUPPLEMENTAL EXPERIMENTAL PROCEDURES

Animals

To generate *Avp-CK1δ^{-/-}* mice, *Avp-Cre* mice [14] were mated to mice with a conditional *CK1δ* allele (*CK1δ^{flox2}*) [3] (N>12 backcrossed to C57BL/6J, The Jackson Laboratory # 010487). Mice were maintained under a strict 12-hour light:dark cycle in a temperature- and humidity-controlled room and fed *ad libitum*. All experimental procedures involving animals were approved by the appropriate institutional animal care and use committee of Kanazawa University.

Behavioral Analyses

Male and female *Avp-CK1δ^{-/-}* (*Avp-Cre;CK1δ^{flox2/flox2}*) and control (*CK1δ^{flox2/flox2}* and *Avp-Cre;CK1δ^{+flox2}*); because these two behaved similarly, we regarded them together as control, Table S1) mice, aged 6 to 19 weeks, were housed individually in a cage placed in a light-tight chamber (light intensity was approximately 50 lux). Spontaneous locomotor activity was monitored by infrared motion sensors (O'Hara) in 1-min bins. Actogram, activity profile, and χ^2 periodogram analysis was performed via ClockLab (Actimetrics). The free-running period was measured by periodogram, as well as by visual inspection, for days 5-19 in DD. The activity time was calculated from the daily activity profile (average pattern of activity) of the same 15 days using the mean activity level as a threshold for detecting the onset and the offset of activity time [14], or by visual inspection. To determine the light-induced phase shift of locomotor activity, animals in their home cages free-running in DD were exposed to a 30-min pulse of white light (approximately 50 lux) at CT14 or CT22. The onset and end of nocturnal activity were determined by visual inspection on actograms for measuring light-induced phase shifts of activity and the number of days required for reentrainment after abrupt shifts in the LD cycles.

Generation and focal injection of recombinant AAV vectors

The AAV-2 ITR-containing plasmid *pAAV-DIO-hChR2(H134R)-EYFP-WPRE-pA* (provided by Dr. Karl Deisseroth) was modified to construct *pAAV-EF1α-DIO-CK1δ* by replacing *hChR2(H134R)* cDNA with mouse *CK1δ* (variant 1) cDNA fragment amplified by PCR from the plasmid *pcFLAG-CK1δ* [S1] (provided by Dr. Isamu Kameshita) using following primers: 5'- attgctagccaccATGgagctgagggtcggggaacagg-3' and 5'- attggcgcgcTCAtcgggtgcacgacagactgaag-3'.

Recombinant AAV vectors expressing *CK1δ* (AAV-DIO-*CK1δ*) or *mCherry* (AAV-DIO-*mCherry*) in a Cre-dependent manner were produced using a triple-transfection, helper-free method and purified as described previously [14]. The titers of recombinant AAV vectors were determined by quantitative PCR: AAV-DIO-*CK1δ*, 8.8×10^{12} ; and AAV-DIO-*mCherry*, 1.0×10^{13} genome copies/ml.

We injected the mixture of AAV-DIO-*CK1δ* and AAV-DIO-*mCherry* (ratio 5:1) into the SCN of eight *Avp-CK1δ^{-/-}* mice so that we could evaluate the efficiency and specificity of expression by immunostaining of mCherry. The stereotaxic injection of AAV vectors was performed as described previously [14]. One week after surgery, mice started to be monitored for their locomotor activity.

Histological Study

Animals were sacrificed by transcardial perfusion of PBS followed by 4% paraformaldehyde fixative. Serial coronal brain sections (30 μ m thick) were collected in four series. One of these was further immunostained or in situ hybridized. Immunostaining was performed as previously described [S2]. The AAV-mediated expression of mCherry was detected by staining with rabbit anti-DsRed (Clontech, 1:2000), biotinylated anti-rabbit antibody (Vector Labs, 1:500), and the Vectastain ABC kit (Vector Labs). Double-immunostaining of AVP and VIP was performed with rabbit anti-AVP (Millipore, 1:2000); goat anti-VIP (Santa Cruz, 1:1000); Alexa 488-conjugated Donkey anti-rabbit IgG (Molecular Probes, 1:2000); and Alexa 594-conjugated Donkey anti-goat IgG (Molecular Probes, 1:2000).

In situ hybridization was performed as previously described using antisense riboprobes labeled with digoxigenin-UTP [S3]. Both *CK1δ^{flox2/flox2}* and *Avp-Cre;CK1δ^{+flox2}* were used as control mice. Antisense riboprobes were synthesized from plasmids containing mouse *Per1* (NM_011065, nucleotides 3443-4515), mouse *Avp* (BC051997, nucleotides 337-531), and mouse *CK1δ* (variant 1, NM_139059, nucleotide 435-1573) cDNAs. The mRNA expression levels were quantified by Photoshop (Adobe) as follows. First, the

images were transformed to grayscale. Then, mean intensities of pixels within the region of interest were calculated. The values of the region adjacent to the SCN were regarded as background and were subtracted from those of the SCN.

Bioluminescence Imaging

The *Avp-CK1 δ 1^{-/-}* mice were further mated with *Per2::Luc* reporter mice [17] (*Avp-Cre;CK1 δ ^{flox2/flox2};Per2::Luc*) and compared to control mice (*CK1 δ ^{flox2/flox2};Per2::Luc*). Mice aged 10 to 17 weeks were housed in DD for 6 days before sampling. Coronal SCN slices of 150 μ m were made at approximately CT8–9 with a vibratome (Leica, Vi1000S). The SCN tissue was dissected at the mid-rostrocaudal region and a paired SCN was cultured on a Millicell-CM culture insert (Millipore) in a sealed dish containing 1.2 mL of DMEM (Invitrogen) supplemented with 10 mM Hepes, 2.74 mM NaHCO₃, 0.1 mM D-luciferin K salt, 2% B27, and 20 mg/L kanamycin at 37°C, as described previously with slight modifications [33].

In a mini-incubator (Tokai Hit) installed on the stage of an inverted microscope (Nikon, Ti-U), PER2::LUC bioluminescence was measured with a 10x objective lens (N.A. 0.45; Nikon) and an EMCCD camera (Andor, iXon3) mounted at the bottom port of the microscope with a 0.7x relay lens. Images were acquired every 30 min with an exposure time of 25 min for 5 days and were analyzed using ImageJ and custom-made program [20]. Resolution of images was adjusted to 4.6 μ m/pixel for further analyses. Circular regions of interest were defined in the shell and core of SCN. Bioluminescence values within the defined regions were detrended by subtracting 24-hr moving average values and then were smoothed with a five-point moving average method. Because the waveforms of luminescence from the SCN shell of *Avp-CK1 δ 1^{-/-};Per2::Luc* mice was noisy in some cases, the middle of the time points crossing value 0 upward and downward were defined as acrophases, and the intervals between two adjacent acrophases were calculated as the periods [14]. We note that very similar results were also obtained when the acrophases were defined as the time points with the maximal values within each cycle.

For pixel-based analyses, we detrended PER2::LUC oscillations in individual pixels for 3 days (data for 72 hr from the first CT6 after slice preparation, determined according to the behavioral free-running period prior to slice preparation) and cosine curve-fitted them using a custom-made program [14, 20] with minor modifications. Pixels with non-significant Pearson correlation coefficients, shown as black pixels, were eliminated to calculate the mean of amplitude (peak-trough difference), period, and first acrophase (peak phase). Pixels with significant oscillation ($p < 0.01$) of periods longer than 34 hr, indicated as white pixels in period maps, were eliminated to calculate the mean period. For the first acrophase, “6 hr” corresponds to the beginning of cosine curved-fitted data (~CT6). The shell and core were defined as pixels within the dorsal 40% or ventral 30% region for individual bilateral SCNs.

Statistical Analysis

All results are expressed as mean \pm SEM. For comparisons of two groups of normally distributed data in the analyses of behavior rhythm, Student's t tests were performed, whereas for comparisons of four groups of normally distributed data, Kruskal-Wallis tests followed by Steel-Dwass post hoc tests were performed. To analyze mRNA expression, two-way repeated-measures ANOVA followed by post hoc Student's t tests or paired t tests were performed. For PER2::LUC imaging, two-way repeated-measures ANOVA was followed by post hoc tests as below. To compare the two groups, Student's t tests or paired t tests were performed; Welch's t test was used when the variances of the two groups differed significantly. To compare the three groups in Figure S3, Friedman tests followed by Wilcoxon signed-rank tests were performed. All p values less than 0.05 were considered to be statistically significant. Only relevant information from statistical analysis is indicated in the text, figures, and tables. Statistical analyses were performed with ANOVA4 and EZR (Saitama Medical Center, Jichi Medical University, Saitama, Japan). The EZR is a graphical user interface for R (The R Foundation for Statistical Computing, Vienna, Austria) [S4]. More precisely, it is a modified version of R commander designed to add statistical functions frequently used in biostatistics.

SUPPLEMENTAL REFERENCES

- S1. Sugiyama, Y., Hatano, N., Sueyoshi, N., Suetake, I., Tajima, S., Kinoshita, E., Kinoshita-Kikuta, E., Koike, T., and Kameshita, I. (2010). The DNA-binding activity of mouse DNA methyltransferase 1 is regulated by phosphorylation with casein kinase 1delta/epsilon. *Biochem J* 427, 489-497.
- S2. Hasegawa, E., Yanagisawa, M., Sakurai, T., and Mieda, M. (2014). Orexin neurons suppress narcolepsy via 2 distinct efferent pathways. *J Clin Invest* 124, 604-616.
- S3. Mieda, M., Williams, S.C., Richardson, J.A., Tanaka, K., and Yanagisawa, M. (2006). The dorsomedial hypothalamic nucleus as a putative food-entrainable circadian pacemaker. *Proc. Natl. Acad. Sci. USA*. 103, 12150-12155.
- S4. Kanda, Y. (2013). Investigation of the freely available easy-to-use software 'EZR' for medical statistics. *Bone Marrow Transplant* 48, 452-458.